INTERNATIONAL JOURNAL FOR NUMERICAL METHODS IN FLUIDS, VOL. 14, 379–401 (1992)

THE APPLICATION OF THE METHOD OF CHARACTERISTICS FOR THE SIMULATION OF NEARLY HORIZONTAL FLOW IN TWO AND THREE SPATIAL DIMENSIONS

P. F. C. MATSOUKIS

Department of Hydraulics, School of Engineering, Democritus University of Thrace, Xanthi 67100, Greece

SUMMARY

Certain free surface flows exhibit in nature negligible vertical accelerations and as a result the pressure within the fluid remains hydrostatic. The method of characteristics is developed as a solution technique for the integration of the partial differential equations describing this kind of flow. The equations are integrated over the depth to provide a two-dimensional model which is then tested and validated by comparing its results with tide-induced flows occurring in a number of cases where either analytical or observational data are available for comparison. On the basis of the results of the 2D model, a finite difference 3D model is developed which provides the values of the unknown velocities u, v and w along the three axes x, y and z. This combined 2D–3D model is verified by applying it in cases of wind-induced flow inside closed or open basins for which the classical Ekman solution may be used as a testing means.

KEY WORDS Characteristics Currents Finite difference techniques Three-dimensional modelling Tides Wind-induced flow

INTRODUCTION

There are certain flow occurrences in nature which exhibit negligible vertical accelerations compared with gravity and as a result operate in an almost horizontal plane. In such a case the equation of momentum conservation along the z-axis leads to a hydrostatic pressure distribution within the fluid. Thus the general partial differential equation system describing the nearly horizontal flow of an incompressible and homogeneous fluid becomes

$$\frac{\partial u}{\partial x}+\frac{\partial v}{\partial y}+\frac{\partial w}{\partial z}=0 \quad \text{(continuity)},$$

$$\left.\begin{aligned}\frac{\mathrm{D}u}{\mathrm{D}t}&=-g\frac{\partial \zeta}{\partial x}+\frac{\partial}{\partial x}\left(A_x\frac{\partial u}{\partial x}\right)+\frac{\partial}{\partial y}\left(A_y\frac{\partial u}{\partial y}\right)+\frac{\partial}{\partial z}\left(A_z\frac{\partial u}{\partial z}\right)+\Omega v\\ \frac{\mathrm{D}v}{\mathrm{D}t}&=-g\frac{\partial \zeta}{\partial y}+\frac{\partial}{\partial x}\left(A_x\frac{\partial v}{\partial x}\right)+\frac{\partial}{\partial y}\left(A_y\frac{\partial v}{\partial y}\right)+\frac{\partial}{\partial z}\left(A_z\frac{\partial v}{\partial z}\right)-\Omega u\end{aligned}\right\} \quad \text{(momentum)}, \tag{1}$$

where x, y and z are Cartesian co-ordinates, t is the time variable, u, v and w are the particle velocities along the axes x, y and z respectively, ζ is the surface elevation above the mean level (Figure 1), A_x, A_y and A_z are eddy viscosity coefficients, g is the acceleration due to gravity, Ω is

0271–2091/92/040379–23$11.50

Received November 1990
Revised April 1991

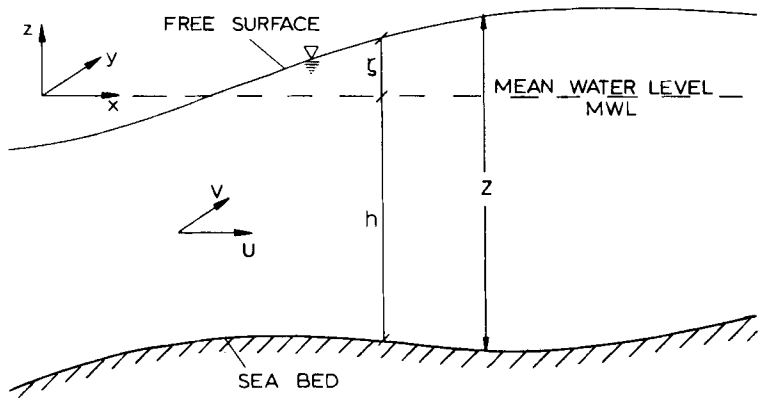

Figure 1. Co-ordinate system and basic notation

the Coriolis parameter ($\Omega = 2\omega \sin\psi$, where $\omega = 0.000073$ rad s^{-1} is the angular frequency of the earth's rotation and ψ is the latitude) and $\mathrm{D}/\mathrm{D}t = \partial/\partial t + u\partial/\partial x + v\partial/\partial y + w\partial/\partial z$ is the total derivative.

The equations above may be integrated over the depth using the appropriate boundary conditions at the bottom and the free surface, giving eventually the following result:

$$\frac{\partial \zeta}{\partial t} + \frac{\partial}{\partial x}[U(h+\zeta)] + \frac{\partial}{\partial y}[V(h+\zeta)] = 0,$$

$$\frac{\partial U}{\partial t} + U\frac{\partial U}{\partial x} + V\frac{\partial U}{\partial y} = -g\frac{\partial \zeta}{\partial x} + \frac{\partial}{\partial x}\left(D_x\frac{\partial U}{\partial x}\right) + \frac{\partial}{\partial y}\left(D_y\frac{\partial U}{\partial y}\right) + \Omega V + \frac{\tau_{sx}}{\rho(h+\zeta)} - \frac{\tau_{bx}}{\rho(h+\zeta)},$$

$$\frac{\partial V}{\partial t} + U\frac{\partial V}{\partial x} + V\frac{\partial V}{\partial y} = -g\frac{\partial \zeta}{\partial y} + \frac{\partial}{\partial x}\left(D_x\frac{\partial V}{\partial x}\right) + \frac{\partial}{\partial y}\left(D_y\frac{\partial V}{\partial y}\right) - \Omega U + \frac{\tau_{sy}}{\rho(h+\zeta)} - \frac{\tau_{by}}{\rho(h+\zeta)}, \qquad (2)$$

where h is the mean water depth (Figure 1), ρ is the sea water density,

$$U = \frac{1}{h+\zeta}\int u\,\mathrm{d}z \quad \text{and} \quad V = \frac{1}{h+\zeta}\int v\,\mathrm{d}z$$

are the depth-integrated velocities, τ_{sx} and τ_{sy} are the shear stress components at the free surface along the axes x and y respectively, τ_{bx} and τ_{by} are the corresponding shear stress components at the bottom and D_x and D_y are eddy diffusivity coefficients taking into account not only the horizontal diffusion of momentum but also the non-uniformity of the velocity over the depth, the so-called 'shear' effect.

This is introduced in the equations by the depth integration of the non-linear convective terms on the left-hand side of equations (1). Indeed, if we assume that the velocities u and v are represented as the sum of the mean values U and V and the residual terms u' and v', then for the first of the momentum equations (1) we have for example

$$\int u\frac{\partial u}{\partial x}\mathrm{d}z+\int v\frac{\partial u}{\partial y}\mathrm{d}z=\int(U+u')\frac{\partial}{\partial x}(U+u')\mathrm{d}z+\int(V+v')\frac{\partial}{\partial x}(U+u')\mathrm{d}z$$
$$=U\frac{\partial U}{\partial x}+V\frac{\partial U}{\partial y}+\frac{\partial}{\partial x}\int u'u'\,\mathrm{d}z+\frac{\partial}{\partial x}\int u'v'\,\mathrm{d}z$$
$$=U\frac{\partial U}{\partial x}+V\frac{\partial U}{\partial y}+\frac{\partial}{\partial x}\left(D_x\frac{\partial U}{\partial x}\right)+\frac{\partial}{\partial y}\left(D_y\frac{\partial U}{\partial y}\right),$$

where the products of the residuals u' and v' have been approximated as shear terms, i.e.

$$\int u'u'\,\mathrm{d}z=D_x\frac{\partial U}{\partial x}\qquad\text{and}\qquad\int u'v'\,\mathrm{d}z=D_y\frac{\partial U}{\partial y}.$$

The bottom stress τ_b is usually expressed as a function of the mean velocity in one of the following ways:

(a) linear: $\dfrac{\tau_{bx}}{\rho}=CU$ and $\dfrac{\tau_{by}}{\rho}=CV,$

(b) semilinear: $\dfrac{\tau_{bx}}{\rho}=\dfrac{C}{h}U$ and $\dfrac{\tau_{by}}{\rho}=\dfrac{C}{h}V,$

(c) non-linear: $\dfrac{\tau_{bx}}{\rho}=g\dfrac{U\sqrt{(U^2+V^2)}}{C^2}$ and $\dfrac{\tau_{by}}{\rho}=g\dfrac{V\sqrt{(U^2+V^2)}}{C^2},$ (3)

where C is the friction coefficient.

The surface stress τ_s is usually exerted by the shear of the blowing wind and is expressed as a quadratic function of the wind velocity W, i.e.

$$\frac{\tau_{sx}}{\rho}=C_D WW_x\qquad\text{and}\qquad\frac{\tau_{sy}}{\rho}=C_D WW_y,\tag{4}$$

where C_D is the dimensionless coefficient of wind friction and W_x and W_y are the wind velocity components.

The depth-integrated equations (2) (2D model) are the well-known 'shallow water' equations of nearly horizontal flow under the assumption of hydrostatic pressure and have found widespread use over the years for the simulation of long-wave propagation (tides, storm surge, seiche, tsunamis, etc.). Their numerical integration in both space and time has been carried out more or less successfully by implementing all sorts of numerical techniques (finite difference, finite element, ADI, etc.), although it is true to say that there are still some problems concerning in particular the simulation of the non-linear terms of the equations.[1]

The solution of equations (1) (3D model) is obviously a more intractable task, let alone the considerable amount of computational work involved. However, three-dimensional calculations have already been attempted, starting with the pioneering work of Heaps[2] and followed by Leendertse and Lin,[3] Forristall,[4] Nihoul,[5] Owen,[6] Koutitas and O'Connors,[7] Heaps,[8] Burg *et al.*,[9] Benque *et al.*,[10] Furnes,[11] Davies,[12] etc. A recent collection of relevant papers can be found in Reference 13.

In the following a new finite difference scheme based on the method of characteristics is presented for the integration in both two and three dimensions of the partial differential equations describing a nearly horizontal flow. Two specific cases are examined which comply with the basic assumption of negligible vertical acceleration and hydrostatic pressure, i.e. (a) the

flow induced by the action of tidal forces and (b) the flow induced by the action of wind over sea areas of shallow depth. The first kind of flow is used as a test case for the characteristics 2D scheme, while the second is used for the 3D characteristics scheme.

In the latter case the solution is achieved in two steps. In the first step the 2D model is solved to provide the value of the free surface elevation ζ. In the second step the gradients $\partial\zeta/\partial x$ and $\partial\zeta/\partial y$ are introduced as known quantities in the three-dimensional equations (1), which are then solved to provide the values of u, v and w in the directions x, y and z. This solution procedure relies on the fact that the free surface elevation should be nearly the same whether calculated by a depth-averaged or a purely three-dimensional scheme.[10]

The combined 2D–3D model is tested and validated by comparing its results with known analytical solutions, serving to demonstrate the efficiency of the method of characteristics for the calculation of a nearly horizontal flow in two or three spatial dimensions.

THE METHOD OF CHARACTERISTICS

The fundamentals of the method of characteristics can be found in the classical work of Courant *et al.*[14] Its development as a solution technique for the simulation of equations (2) has been given by Butler[15] and also by Daubert and Graffe.[16] In the following we summarize their main conclusions.

From the mathematical point of view equations (2) form a non-linear hyperbolic system of partial differential equations in three independent variables x, y and t. The main distinction of a hyperbolic system is the existence of characteristics. By definition, a characteristic in m independent variables is a subspace of $m-1$ dimensions across which discontinuities in the solution surface may occur and thus the solution on a characteristic cannot be analytic.

In our case there are three independent variables. Therefore any characteristic surface will depend on two space variables x and y in the functional form $t=\beta(x, y)$ or the equivalent parametric form $x=x(t)$ and $y=y(t)$. In order to establish the function β, we first write the shallow water equations (2) in matrix form as

$$\frac{\partial \mathbf{A}}{\partial t}+\mathbf{A}_1\frac{\partial \mathbf{A}}{\partial x}+\mathbf{A}_2\frac{\partial \mathbf{A}}{\partial y}=\mathbf{B}, \tag{5}$$

where

$$\mathbf{A}=\begin{bmatrix}U\\V\\Z\end{bmatrix}, \qquad \mathbf{A}_1=\begin{bmatrix}U & 0 & g\\0 & U & 0\\Z & 0 & U\end{bmatrix}, \qquad \mathbf{A}_2=\begin{bmatrix}V & 0 & 0\\0 & V & g\\0 & Z & V\end{bmatrix},$$

$$\mathbf{B}=\begin{bmatrix}g\,\partial h/\partial x+F_x\\g\,\partial h/\partial y-F_y\\0\end{bmatrix}, \qquad F_x=\Omega V+\frac{\tau_{sx}}{\rho(h+\zeta)}-\frac{\tau_{bx}}{\rho(h+\zeta)}, \qquad F_y=-\Omega U+\frac{\tau_{sy}}{\rho(h+\zeta)}-\frac{\tau_{by}}{\rho(h+\zeta)}$$

and $Z=h+\zeta$ is the total depth.

Let us assume that the solution of matrix equation (5) is of the type $\mathbf{A}=\mathbf{A}(x, y, t)$ and the solution $\mathbf{A}_0$ at a point $\mathrm{M}(x_0, y_0, t_0)$ lying on a characteristic surface is known. Then $\mathbf{A}(x, y, t)=\mathbf{A}(x, y, \beta(x, y))=\mathbf{A}_0$ and

$$\frac{\partial \mathbf{A}_0}{\partial x}=\frac{\partial \mathbf{A}}{\partial x}+\frac{\partial \mathbf{A}}{\partial t}\frac{\partial \beta}{\partial x}, \qquad \frac{\partial \mathbf{A}_0}{\partial y}=\frac{\partial \mathbf{A}}{\partial y}+\frac{\partial \mathbf{A}}{\partial t}\frac{\partial \beta}{\partial y}. \tag{6}$$

Equations (5) and (6) comprise a system of three equations in three unknowns, i.e. the derivatives of the solution surface at the point M, $\partial\mathbf{A}/\partial x$, $\partial\mathbf{A}/\partial y$ and $\partial\mathbf{A}/\partial t$. This system must have no solution, otherwise an analytical solution could be established in the neighbourhood of M using, for example, the values of these derivatives and a Taylor formula. This would contradict the basic assumption that M lies on a characteristic surface. In this respect equations (5) and (6) may be rewritten as

$$\mathbf{R}\mathbf{X}=\mathbf{Y}, \tag{7}$$

where

$$\mathbf{R}=\mathbf{I}-\mathbf{A}_1\frac{\partial\beta}{\partial x}-\mathbf{A}_2\frac{\partial\beta}{\partial y}, \qquad \mathbf{X}=\frac{\partial\mathbf{A}}{\partial t}, \qquad \mathbf{Y}=\mathbf{B}-\mathbf{A}_1\frac{\partial\mathbf{A}_0}{\partial x}-\mathbf{A}_2\frac{\partial\mathbf{A}_0}{\partial y}$$

and $\mathbf{I}$ is the unit matrix. The solution is undefined only if $\mathbf{R}$ is singular and its determinant $|\mathbf{R}|$ is equal to zero, i.e.

$$|\mathbf{R}|=\begin{vmatrix} 1-Up-Vq & 0 & -gp \\ 0 & 1-Up-Vq & -gq \\ -Zp & -Zq & 1-Up-Vq \end{vmatrix}=0,$$

where $p=\partial\beta/\partial x$ and $q=\partial\beta/\partial y$. By solving, we obtain

$$(1-Up-Vq)^2-gZ(p^2+q^2)=0, \qquad 1-Up-Vq=0. \tag{8}$$

Since p and q are obviously the components of the normal to the surface β, each of the relationships above defines a characteristic surface. By confining the solution locally, the characteristic surfaces may be replaced by the tangential planes $t=px+qy$ passing through point M.

If $p=\rho\cos\varphi$ and $q=\rho\sin\varphi$, then the first equation of (8) defines the tangential plane $(x-Ut)\cos\varphi+(y-Vt)\sin\varphi=\sqrt{(gZ)}t$ or by differentiation $-\sin\varphi(x-Ut)+\cos\varphi(y-Vt)=0$. Eliminating φ between these two, we obtain

$$(x-Ut)^2+(y-Vt)^2=a^2t^2, \tag{9}$$

where $a=\sqrt{(gZ)}$ is the wave speed.

This equation defines geometrically the so-called 'characteristic cone' having the differential form

$$\frac{\mathrm{d}x}{\mathrm{d}t}=U+a\cos\varphi, \qquad \frac{\mathrm{d}y}{\mathrm{d}t}=V+a\sin\varphi, \tag{10}$$

where φ is the parametric angle measured anticlockwise (Figure 2). Each value of φ defines a generator, i.e. a 'bicharacteristic' of the characteristics cone.

In a similar way the second equation of (8) leads to the parametric form

$$t=px+\frac{1-Up}{V}y, \tag{11}$$

which represents planes rotating around the line

$$\frac{\mathrm{d}x}{\mathrm{d}t}=U, \qquad \frac{\mathrm{d}y}{\mathrm{d}t}=V. \tag{12}$$

This is in fact the axis of the characteristic cone and defines the path followed by an individual particle in a Lagrangian sense, i.e. the so-called 'particle path' line.

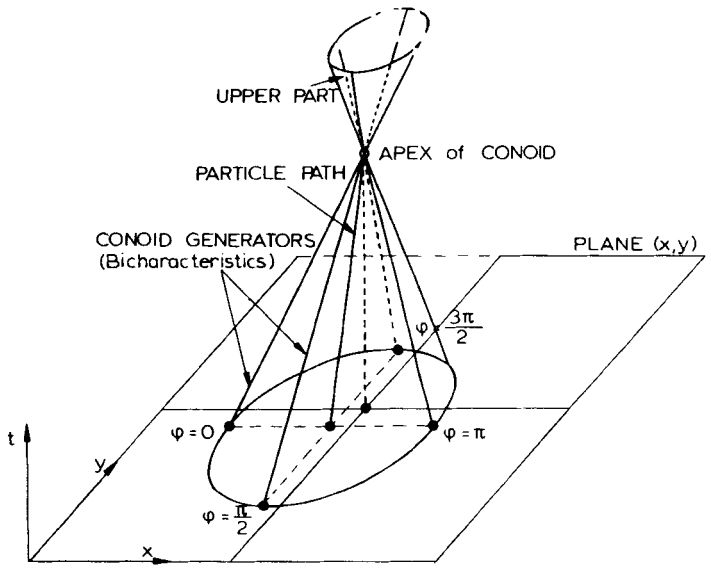

Figure 2. Characteristics cone and particle path line

Given that **R** is singular, equations (5) and (6) are not linearly independent. Therefore there must exist a matrix **L** with elements l_1, l_2 and l_3 such that

$$\mathbf{LR}=0, \qquad \mathbf{LY}=0. \tag{13}$$

The first equation of (13) is used to define the matrix **L** and the second is used to define the condition holding along a characteristic surface.

In the case of the characteristics cone the condition $\mathbf{LR}=0$ leads to the values $l_1=a(\cos\varphi)/g$, $l_2=a(\sin\varphi)/g$ and $l_3=1$. Thus the condition holding on any characteristic at angle φ takes the form

$$g\frac{\mathrm{d}Z}{\mathrm{d}t}+a\cos\varphi\frac{\mathrm{d}U}{\mathrm{d}t}+a\sin\varphi\frac{\mathrm{d}V}{\mathrm{d}t}=f, \tag{14}$$

$$f=ag\left(\frac{\partial h}{\partial x}\cos\varphi+\frac{\partial h}{\partial y}\sin\varphi\right)-a^2\left[\frac{\partial U}{\partial x}\sin^2\varphi-\left(\frac{\partial U}{\partial y}+\frac{\partial V}{\partial x}\right)\sin\varphi\cos\varphi+\frac{\partial V}{\partial y}\cos^2\varphi\right]$$
$$+aF_x\cos\varphi+aF_y\sin\varphi.$$

In the case of the particle path line it is found in a similar way that $l_1=l_2=0$ and $l_3=1$. Thus the equivalent characteristic condition is

$$g\frac{\mathrm{d}Z}{\mathrm{d}t}=-a^2\left(\frac{\partial U}{\partial x}+\frac{\partial V}{\partial y}\right). \tag{15}$$

This is simply the continuity equation after rearranging its terms and therefore it can be seen that the particle path does not lead to a genuine characteristic condition in the same way as the bicharacteristics of the characteristics cone.

FINITE DIFFERENCE SCHEME

The region under consideration is divided in space and time (Figure 3) to give a network of solution points with co-ordinates $i\Delta x$ and $j\Delta y$ (Δx and Δy are space increments along the axes x and y respectively and i and j are integers) where both the velocities U and V and the elevation ζ are calculated at each time step $n\Delta t$ (Δt is a time increment and n is an integer). Only values of the variables lying on the previous time plane are used in the solution. Thus an explicit-type scheme is employed over a non-staggered grid of discrete points.

Considerations of numerical stability and accuracy of the scheme suggest the use of the characteristic conditions (14) at specific values of the angle φ for the construction of the solution, i.e. $\varphi = 225°$, 315°, 45° and 135°, and also along the particle path line.[17] All the bicharacteristics are projected backwards in time to intersect the previous time plane at $t - \Delta t$, defining thereby the co-ordinates of intersection points 1–5 (Figure 4) relative to the grid point of solution 0, i.e.

$$
\begin{aligned}
X5 &= -U\Delta t, & Y5 &= -V\Delta t,\\
X1 &= X5 + a(\cos 45)\Delta t, & Y1 &= Y5 + a(\sin 45)\Delta t,\\
X2 &= X5 - a(\cos 45)\Delta t, & Y2 &= Y5 + a(\sin 45)\Delta t,\\
X3 &= X5 - a(\cos 45)\Delta t, & Y3 &= Y5 - a(\sin 45)\Delta t,\\
X4 &= X5 + a(\cos 45)\Delta t, & Y4 &= Y5 - a(\sin 45)\Delta t,
\end{aligned}
\tag{16}
$$

where points 1–4 are the intersection points of the four bicharacteristics with the time plane and point 5 is the intersection of the particle path line (Figure 4). As a first approximation the values of U, V and a at point 0 are used in the expressions above but calculated at the previous time level.

The characteristic conditions (14) along these five characteristic lines contain only total derivatives on their left-hand side and may be directly approximated by forward differences, providing five equations for the construction of the solution in the following way:

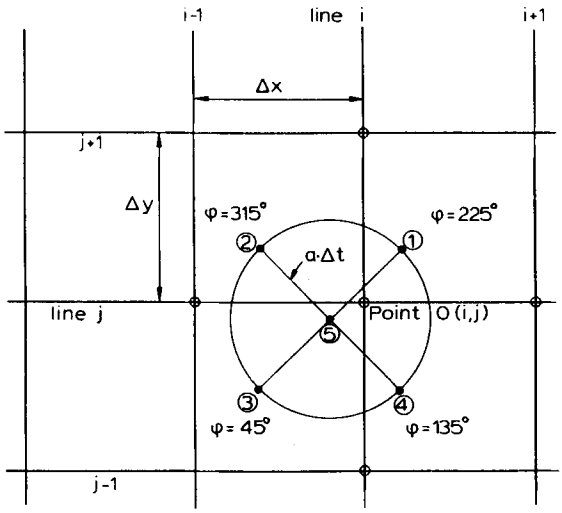

Figure 3. Grid construction and cone projection on (x, y)

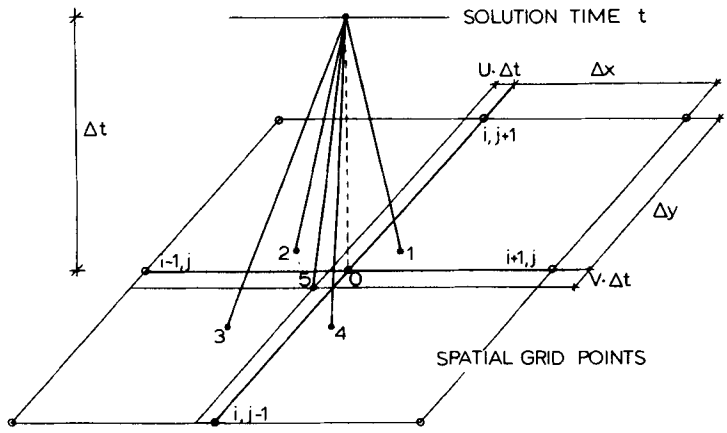

Figure 4. Explicit construction of solution and intersection points 1–5

$$g\frac{Z-Z1}{\Delta t}-a\cos 45\frac{U-U1}{\Delta t}-a\sin 45\frac{V-V1}{\Delta t}=f_1,$$

$$g\frac{Z-Z2}{\Delta t}+a\cos 45\frac{U-U2}{\Delta t}-a\sin 45\frac{V-V2}{\Delta t}=f_2,$$

$$g\frac{Z-Z3}{\Delta t}+a\cos 45\frac{U-U3}{\Delta t}+a\sin 45\frac{V-V3}{\Delta t}=f_3,$$

$$g\frac{Z-Z4}{\Delta t}-a\cos 45\frac{U-U4}{\Delta t}+a\sin 45\frac{V-V4}{\Delta t}=f_4,$$

$$g\frac{Z-Z5}{\Delta t}=-a^2\left(\frac{\partial U}{\partial x}+\frac{\partial V}{\partial y}\right), \tag{17}$$

where Z, U and V are the integrated variables located at the apex of the conoid, $Z1$, $Z2$, $U1$, $U2$, etc. are the values of the variables at intermediate points 1–5 and f_1, f_2, f_3 and f_4 are the values of the quantity f at points 1–4.

By combining equations (17), partial derivatives are eliminated and the final solution takes the simple form

$$\zeta=\frac{R1+R2+R3+R4}{2}-\zeta_5,$$

$$U=\frac{R2+R3-R1-R4}{4a}(\sqrt{2})g+F_x\Delta t,$$

$$V=\frac{R3+R4-R1-R2}{4a}(\sqrt{2})g+F_y\Delta t, \tag{18}$$

where the quantities $R1$–$R4$ (Riemann invariants) are all calculated at the previous time level as

$$R1=\zeta_1-\frac{\sqrt{2}}{2}\frac{a}{g}U1-\frac{\sqrt{2}}{2}\frac{a}{g}V1,$$

$$R2=\zeta_2+\frac{\sqrt{2}}{2}\frac{a}{g}U2-\frac{\sqrt{2}}{2}\frac{a}{g}V2,$$

$$R3=\zeta_3+\frac{\sqrt{2}}{2}\frac{a}{g}U3-\frac{\sqrt{2}}{2}\frac{a}{g}V3,$$

$$R4=\zeta_4-\frac{\sqrt{2}}{2}\frac{a}{g}U4-\frac{\sqrt{2}}{2}\frac{a}{g}V4, \tag{19}$$

and ζ_1, ζ_2, etc. are the values of the elevation ζ at points 1–5.

The calculation of any variable at these points is carried out by means of an interpolating scheme which is equivalent to a Taylor formula taken up to second-oder accuracy. Accordingly, the value $Q_{x,y}$ of any quantity Q at a point (x, y) of the network will be

$$Q_{x,y}=Q_{i,j}+xL_x(Q)+0{\cdot}5x^2L_{xx}(Q)+yL_y(Q)+0{\cdot}5y^2L_{yy}(Q), \tag{20}$$

where $Q_{i,j}$ is the value of Q at a point of solution $O(i\Delta x, j\Delta y)$ known from the previous time level and L_x, L_y, L_{xx}, etc. are finite difference operators:

$$L_x(Q)=\frac{Q_{i+1,j}-Q_{i-1,j}}{2\Delta x}, \qquad L_y(Q)=\frac{Q_{i,j+1}-Q_{i,j-1}}{2\Delta y},$$

$$L_{xx}(Q)=\frac{Q_{i+1,j}+Q_{i-1,j}-2Q_{i,j}}{\Delta x\,\Delta x},$$

$$L_{yy}(Q)=\frac{Q_{i,j+1}+Q_{i,j-1}-2Q_{i,j}}{\Delta y\,\Delta y}. \tag{21}$$

As a result the final solution (18) is expressed in terms of the values of the variables ζ, U and V at grid points only.

Two kinds of boundary points are recognized within the model area: those lying along the coastline (closed boundary points) and those on a line connecting with the open sea (open boundary points). At closed boundary points U or V (or both) is taken as zero depending on the orientation of the boundary line inside the model, while along the open boundary points specific conditions must be applied according to the nature of the problem at hand. For example, if tidal flow is simulated, then the surface elevation is usually prescribed at the open boundary as a sinusoidal function of time, i.e. $\zeta=A\cos(\sigma t)$, where A is the wave amplitude, $\sigma=2\pi/T$ is the angular frequency and T is the tidal period.

The space increment is usually taken in practical applications to be the same along the x- and y-axis, i.e. $\Delta x=\Delta y=\Delta s$.

Furthermore, if accuracy analysis is carried out, the solution scheme of equations (18) is found to be of second-order accuracy in both space and time, while stability analysis imposes the following two criteria for the numerical stability of the scheme:

(a) $$\frac{U^2+V^2+2a^2}{\sqrt{[(a\sqrt{2}-U-V)^2-4UV]}}\Delta t\leqslant\Delta s, \tag{22}$$

(b) $$\Delta t=\frac{2C}{\Omega^2+C^2}, \tag{23}$$

where C is a linear friction coefficient for the bottom shear stress (equations (3)).

Condition (a) reduces to the well-known CFL criterion for stability,

$$\frac{a\Delta t}{\Delta s} \leqslant \frac{1}{\sqrt{2}}, \tag{24}$$

if the non-linear convective terms on the left-hand side of equations (2) are omitted.

TIDAL FLOW

The periodical phenomenon of tides is now used to check the efficiency and accuracy of the proposed characteristics scheme (equations (18)) for the simulation of the two-dimensional, depth-averaged, nearly horizontal flow. This is necessary because the scheme will be used *inter alia* for the solution of the three-dimensional equations (1) as well. This is demonstrated in the following section.

The tidal waves generated in nature by the action of the planetary forces exhibit extremely long periods and wavelengths. As a result their propagation, even in regions of large water depths, takes place in an almost horizontal plane and under 'shallow water' conditions, which means that the fluid pressure remains virtually hydrostatic. Therefore the mathematical description of such a propagation in two spatial dimensions is adequately provided through equations (2).

The tidal flow established inside a straight, orthogonal channel of constant depth with a reflecting wall at its end may be used as a first elementary test case for the characteristics scheme (18), since the solution in this case is a simple standing wave of elevation

$$\zeta = 2A\cos(kx)\cos(\sigma t), \tag{25}$$

where A is the tidal amplitude at the entrance of the channel, $\sigma = 2\pi/T$ is the angular frequency of the tide, x is the distance measured from the end towards the mouth of the channel and $k = 2\pi/L$ is the wave number.

Under linear conditions and without taking into account free surface and bottom friction stress and the Coriolis effect, equations (18) become in finite difference form

$$\begin{aligned}
\zeta_{i,j}^{n+1} &= \zeta_{i,j}^{n} + \frac{a^2\Delta t^2}{2} L_{xx}(\zeta^n) + \frac{a^2\Delta t^2}{2} L_{yy}(\zeta^n) - h\,\Delta t\,[L_x(U^n) + L_y(V^n)], \\
U_{i,j}^{n+1} &= U_{i,j}^{n} + \frac{a^2\Delta t^2}{2} L_{xx}(U^n) + \frac{a^2\Delta t^2}{2} L_{yy}(U^n) - g\,\Delta t\,L_x(\zeta^n), \\
V_{i,j}^{n+1} &= V_{i,j}^{n} + \frac{a^2\Delta t^2}{2} L_{xx}(V^n) + \frac{a^2\Delta t^2}{2} L_{yy}(V^n) - g\,\Delta t\,L_y(\zeta^n).
\end{aligned} \tag{26}$$

Starting with initial tidal elevations those of the analytical solution above at HW time, equations (26) produce numerical elevations which are very close to the analytical values of (25) (Figure 5). The other details of the applied scheme are as follows: $\Delta s = 1965$ m, $\Delta t = 162$ s, $A = 2$ m, $h = 15$ m. As is also predicted by (25) above, the numerical scheme verifies that there is no phase lag in the solution, HW elevations occurring simultaneously along the length of the channel.

However, it seems that the analytical solution developed by Lynch and Gray[18] for the tidal flow occurring in channels of a quarter-annular configuration and a bathymetry varying according to $h = h_0 r^n$, where h_0 is a constant, r is the radial distance and n is an integer (Figure 6), has become the standard test case for the performance of numerical schemes of any kind solving the two-dimensional tidal equations.

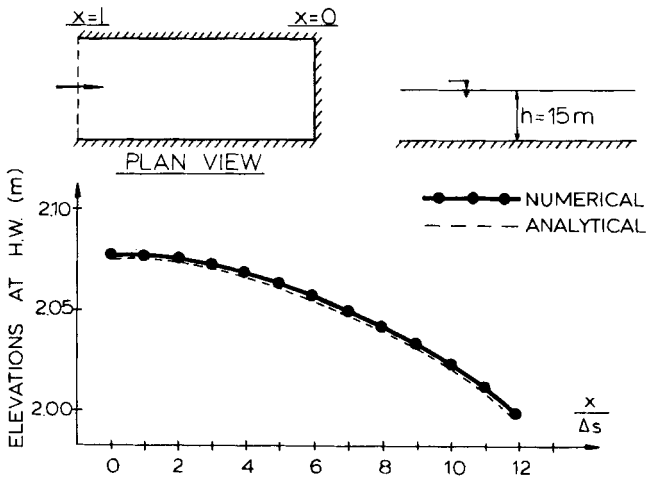

Figure 5. Tidal wave in an orthogonal channel of constant depth

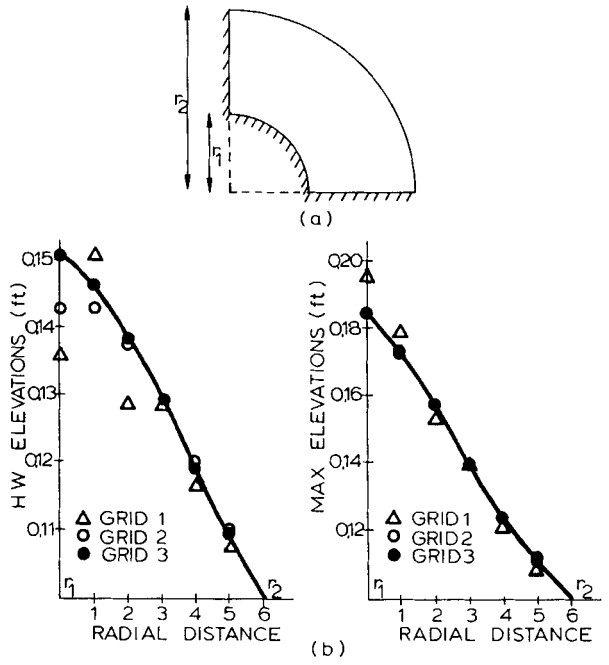

Figure 6. Channel of quarter-annular configuration and quadratically varying depth—HW and maximum elevations along a radius

For comparison reasons, the test cases employed by Lynch and Gray[19] have been adopted herein referring to three different sea bed configurations: (a) a constant depth of 9 m (30 ft) ($n=0$); (b) a linearly varying depth from 6 m (20 ft) at $r=r_1$ to 15 m (50 ft) at $r=r_2$ ($n=1$); (c) a quadratically varying depth from 3 m (10 ft) at r_1 to 18·75 m (62·5 ft) at r_2 ($n=2$). The other details of

the scheme are as follows: $\Delta r = 15$ km (5×10^4 ft), $r_1 = 4\Delta r$, $r_2 = 10\Delta r$, linear friction coefficient $C = 10^{-4}\,s^{-1}$, tidal period $T = 12{\cdot}4$ h, amplitude 0·03 m (0·1 ft) at $r = r_2$.

Three different grid sizes have been tested with a view to demonstrating the convergence qualities of the characteristics numerical scheme: (a) $\Delta s = \Delta r$ (grid 1); (b) $\Delta s = \Delta r/2$ (grid 2); (c) $\Delta s = \Delta r/4$ (grid 3). The stability conditions (22) and (23) were used each time to define the proper value of the time increment Δt.

As expected, the results are found to be circumferentially identical and the numerical solution converges towards the analytical one as the space increment Δs is reduced. In the case of quadratically varying water depth the best performance is achieved with grid 3 either with or without friction (Figures 6 and 7) for both elevations and velocities (Figure 8). In the case of a constant or a linearly varying water depth the analytical solution is already attained with grid 2 (Figure 9).

The ability of the characteristics scheme to describe adequately the main features of a two-dimensional tidal flow is further demonstrated by its application in a case of practical civil engineering interest, i.e. for the simulation of the tide occurring in the Bristol channel, one of the greatest in the world.

The area under consideration, having a maximum water depth of 40 m, is covered by a network of $39 \times 31 = 1209$ grid points using a space increment $\Delta s = 4{\cdot}5$ km. The M_2 tidal constituent is in particular examined and tidal data are interpolated from Tide Tables and Admiralty Charts to be introduced along the open boundary line of the model in the form of a sinusoidal variation of the elevation with the proper phase value. Under these conditions the stability criteria lead to a value of the time increment Δt equal to 81 s, while a universal value of the non-linear Chezy coefficient $C = 30\,m^{1/2}\,s^{-1}$ is applied everywhere in order to simulate correctly the tidal ranges observed, particularly in the shallow waters of the region.

The model must run for a total time of three tidal periods so that a periodic solution is established at the end and this requires a CPU time of 4·5 min on a microVAX II computer.

Numerical results are presented in the form of co-range and co-tidal lines (i.e. lines of equal range and equal tidal phase) and these are favourably compared with observed values provided by British Admiralty Chart No. 5058 (see Figures 10 and 11).

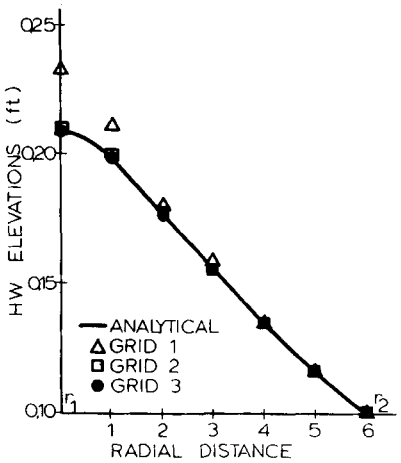

Figure 7. Channel of quarter-annular configuration and quadratically varying depth—frictionless case

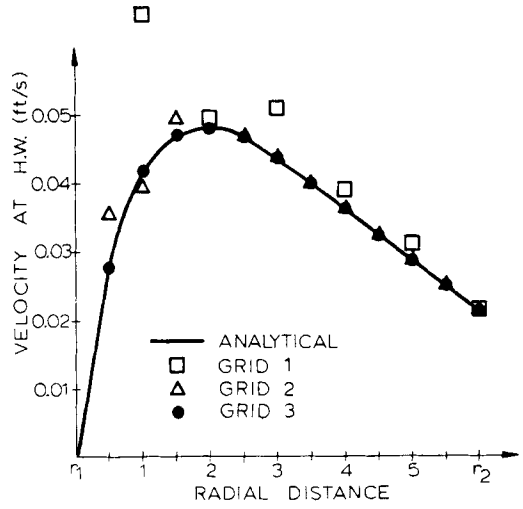

Figure 8. Velocity diagram along a radius—HW time at $r=r_2$

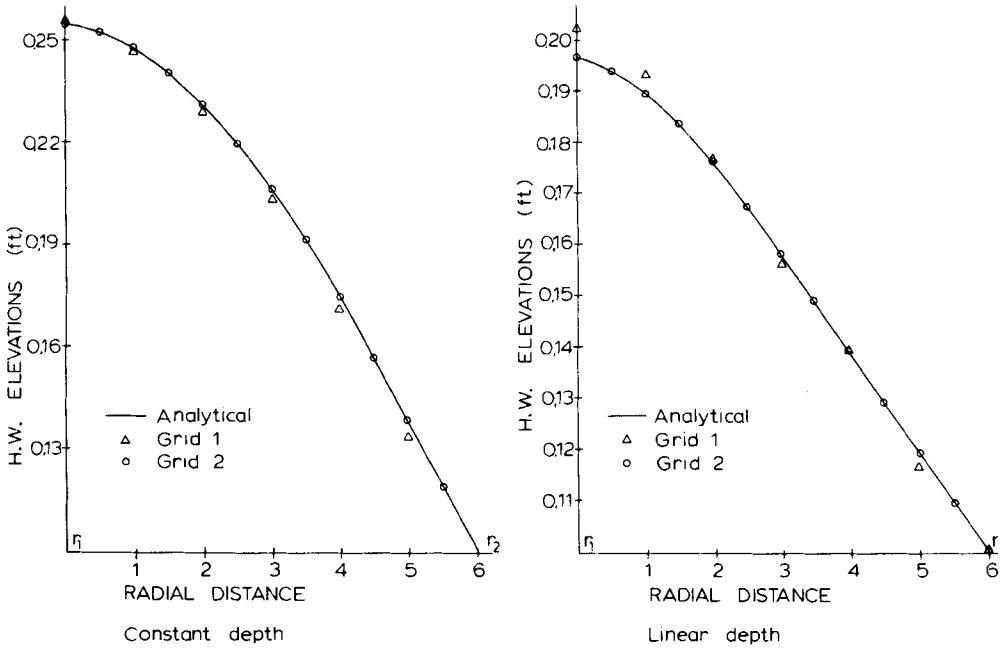

Figure 9. Quarter-annular channel of constant and linear depth—HW elevations

WIND-INDUCED FLOW

The vertical distribution of the tidal current is usually found to have a logarithmic form and thus the relationships established by (3) may be considered as a valid expression of the shear stress at the bottom. However, this is not true for a wind-induced flow, i.e. a flow generated by the wind

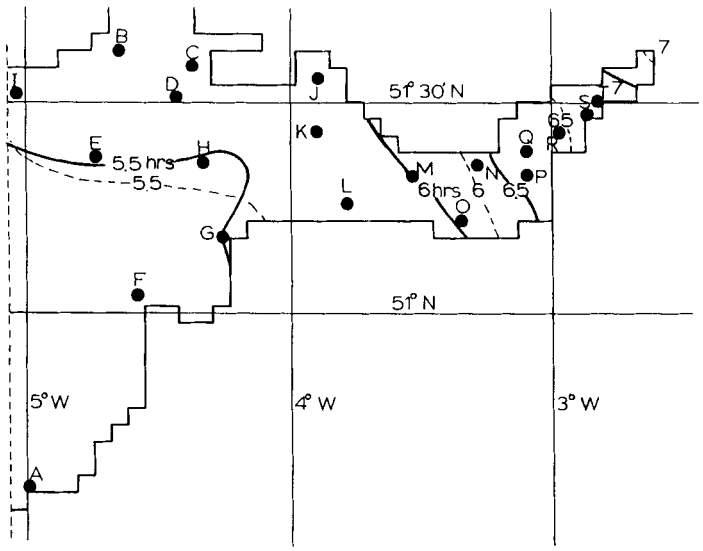

Figure 10. Bristol Channel—isolines of equal HW time: ——, observed; – – –, calculated

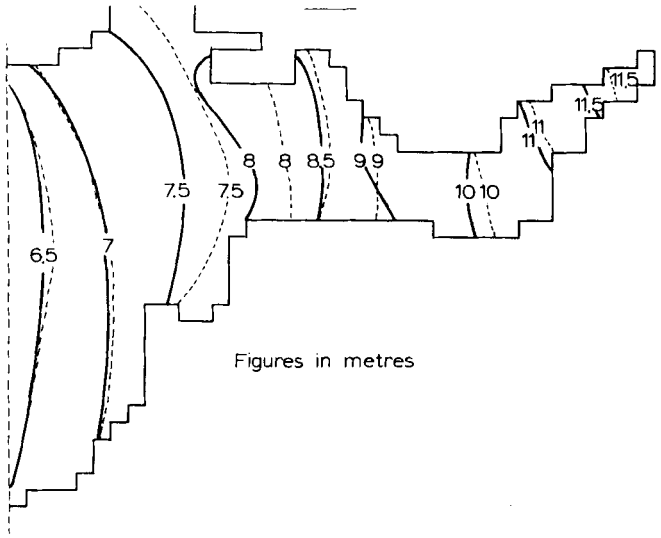

Figure 11. Bristol Channel—isolines of equal tidal range: ——, observed; – – –, calculated

blowing at the free surface, since it is a well-known fact that in such a case a flow reversal takes place along the vertical. Therefore the water masses close to the bottom may be well directed in the opposite sense to the mean flow and under these conditions formulation (3) cannot be considered as a realistic way to simulate the bottom friction effects.

To overcome this problem, the shear stress at the bottom is calculated in this work directly from Newton's law of friction, i.e.

$$\tau_{bx}=A_z\frac{\partial u}{\partial z}, \qquad \tau_{by}=A_z\frac{\partial v}{\partial z}, \tag{27}$$

where the derivatives $\partial u/\partial z$ and $\partial v/\partial z$ are approximated by forward differences using the values of u and v calculated by the 3D model.

The latter takes the following form if the interpolating scheme (20) is introduced in the equations and the eddy viscosity coefficients A_x, A_y and A_z are assumed temporarily as constant:

$$\begin{aligned}
u^{n+1}_{i,j,k}&=u^n_{i,j,k}+\left(\frac{a^2\Delta t^2}{2}+A_x\right)L_{xx}(u^n_{i,j,k})+\left(\frac{a^2\Delta t^2}{2}+A_y\right)L_{yy}(u^n_{i,j,k})\\
&\quad -u_0\Delta t L_x(u^n_{i,j,k})-v_0\Delta t L_y(u^n_{i,j,k})-w_0\Delta t L_z(u^n_{i,j,k})+A_z\Delta t L_{zz}(u^n_{i,j,k})+\Omega\Delta t v_0+\lambda_x\Delta t,\\
v^{n+1}_{i,j,k}&=v^n_{i,j,k}+\left(\frac{a^2\Delta t^2}{2}+A_x\right)L_{xx}(v^n_{i,j,k})+\left(\frac{a^2\Delta t^2}{2}+A_y\right)L_{yy}(v^n_{i,j,k})\\
&\quad -u_0\Delta t L_x(v^n_{i,j,k})-v_0\Delta t L_y(v^n_{i,j,k})-w_0\Delta t L_z(v^n_{i,j,k})+A_z\Delta t L_{zz}(v^n_{i,j,k})+\Omega\Delta t u_0+\lambda_y\Delta t,
\end{aligned} \tag{28}$$

where

$$\begin{aligned}
u_0&=(u^n_{i+1,j,k}+u^n_{i-1,j,k}+u^n_{i,j+1,k}+u^n_{i,j-1,k})/4,\\
v_0&=(v^n_{i+1,j,k}+v^n_{i-1,j,k}+v^n_{i,j+1,k}+v^n_{i,j-1,k})/4,\\
w_0&=(w^n_{i+1,j,k}+w^n_{i-1,j,k}+w^n_{i,j+1,k}+w^n_{i,j-1,k})/4.
\end{aligned}$$

The terms λ_x and λ_y depending on the surface gradient are calculated by means of central finite differences using the solution provided by the two-dimensional scheme (18):

$$\lambda_x=-gL_x(\zeta^n_{i,j}), \qquad \lambda_y=-gL_y(\zeta^n_{i,j}).$$

The vertical velocity w at a depth level z, i.e. $w(z)$, is calculated by integrating the continuity equation as

$$w(z)=-\int_{-h}^{z}\left(\frac{\partial u}{\partial x}+\frac{\partial v}{\partial y}\right)dz, \tag{29}$$

where the derivatives are approximated by central differences using the 3D solution of u and v.

Stability analysis of scheme (28) shows that besides (22) and (23) the following stability criterion involving the vertical eddy viscosity coefficient should also be satisfied:

$$A_z\Delta t\leqslant 0{\cdot}25\Delta z. \tag{30}$$

The conditions which must be necessarily applied at the sea bottom or on any other solid boundary for the solution of the equations depend on the assumed values of the eddy viscosity coefficients.

(1) If A_x, A_y, $A_z\neq 0$, then the no-slip condition is applied, i.e.

$$u=v=w=0. \tag{31}$$

(2) If A_x, A_y or $A_z=0$, then a slip condition is applied using, for example, equations (3), where the values of the mean flow U and V may now be replaced by the values of u and v along the boundary under consideration.

For the calculation of the vertical velocity w a 'rigid lid' assumption is made at the free surface, i.e. $w=0$, or a kinematic boundary condition is implemented through the depth-integrated continuity equation (15), i.e.

$$w=\frac{d\zeta}{dt}=\frac{a^2}{g}\left(\frac{\partial U}{\partial x}+\frac{\partial V}{\partial y}\right). \tag{32}$$

Concluding, the solution of the three-dimensional equations (1) may be seen to proceed in the following way.

1. Solve the depth-averaged model (2) using the two-dimensional characteristics scheme (18) and equation (27) for the calculation of the bottom shear stress. Both the free surface elevation ζ and its gradients $\partial\zeta/\partial x$ and $\partial\zeta/\partial y$ are defined by means of the depth-integrated velocities U and V.
2. Introduce the surface gradient values in the 3D model (28) for the calculation of the values of u, v and w.
3. Using the newly computed values of u and v, calculate the bottom shear stress using (27). This is then introduced in the 2D model (18) (step 1) for use at the next time level and so on.

An elementary test of this combined 2D–3D model may be achieved by confining the problem to two spatial dimensions x and z. In such a case equations (1) take the following very simple form if all non-linear convective, horizontal diffusion and Coriolis terms are omitted:

$$\frac{\partial u}{\partial t}=-g\frac{\partial\zeta}{\partial x}+A_z\frac{\partial^2 u}{\partial z^2}. \tag{33}$$

When a steady state is attained, $\partial u/\partial t=0$, and by introducing the boundary conditions $u=0$ at the bottom and $A_z\partial u/\partial z=C_D W|W|$ at the free surface, an analytical solution can be derived, namely

$$u=C_D W|W|\frac{h}{A_z}\left(0{\cdot}75\frac{\zeta^2}{h^2}+\frac{\zeta}{h}+0{\cdot}25\right). \tag{34}$$

In this respect let us consider an open-ended basin of constant depth $h=10$ m over which a constant wind of 20 m s^{-1} is blowing (Figure 12). The basin is described by 51 points both along the x- and the z-axis with space increments $\Delta x=2{\cdot}83$ m and $\Delta z=0{\cdot}2$ m. The other parameters of the problem are as follows: $A_z=0{\cdot}0158$ m^2 s^{-1}, $C_D=1{\cdot}78\times10^{-6}$, $C=0{\cdot}001$ m$^{1/2}$ s^{-1}.

After a number of iterations the combined 2D–3D model described above leads to a steady state according to which the vertical distribution of the velocity u remains constant along the x-axis and also in time. The numerical solution provided by scheme (28) under the prescribed conditions is compared with the analytical one (equation (34)) in Figure 13, where it can be seen that the two solutions are in fact identical.

Models of this kind are usually validated by comparing their results with the classical Ekman[20]

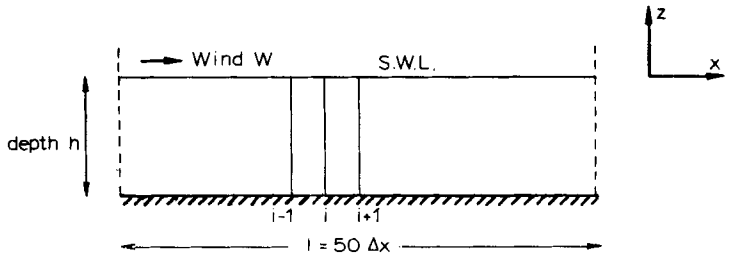

Figure 12. Open basin configuration

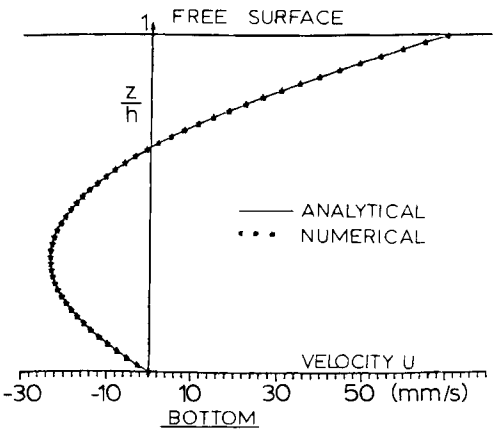

Figure 13. Vertical distribution of velocity U

solution for the wind-induced flow generated inside a closed basin of constant depth and constant eddy viscosity coefficient by the action of a constant wind.

Let us consider, therefore, an orthogonal basin closed on all its sides having a length $L = 200$ km, a width $B = 100$ km and a depth $h = 50$ m (Figure 14). The space increments along the three axes are taken as $\Delta x = \Delta y = 10$ km and $\Delta z = 5$ m, which means that the basin is described by 21×11 points in the horizontal and by 11 points along the vertical. The wind speed is 15 m s^{-1} and the values of the wind, bottom friction and eddy viscosity coefficients C_D, C and A_z are taken the same as before. The required CPU time to achieve a steady state is found to be 3 min on a microVAX II computer.

If the Coriolis term is omitted and a slip condition is applied at the sea bottom by means of a linear law of friction (equation (3)), then an analytical solution of the problem is possible, e.g. the one provided by Jamart and Oser.[21] The numerical solution given by (28) is found to be in very close agreement with this analytical solution as can be seen in Figure 15, where the time variation of the elevation ζ at the boundary point $x = 0$, $y = B/2$ is depicted up to the point of steady state after almost 150 iterations. Obviously, if the value of the space increment Δs is reduced, then a better approximation between the two solutions can be achieved.

It is interesting to comment on the mean velocity, which according to Ekman must be everywhere equal to zero. This velocity is calculated by the 2D model (18) as an unknown variable through its components U and V (equations (2)), but it may also be calculated by the 3D model (28) as the integral of the 3D velocities u and v over the depth (residual velocities). In both cases the mean velocity is found by the numerical scheme to be zero at every point of the grid in accordance with Ekman's theory.

Also according to Ekman, the surface current, drawn in Figure 16, is found to deviate to the right of the wind direction as a result of the Coriolis force action. The angle of deviation is measured as 25° compared with the value of 26° predicted by Ekman, while the maximum current is 0·24 m s^{-1} compared with Ekman's value of 0·25 m s^{-1}.

The isolines of the free surface elevation depicting a constant gradient over the basin are produced by the numerical model with a slight deviation to the right for the same reason as above, i.e. because of the Coriolis effect (Figure 17). If the Coriolis term is omitted from the equations, then the isolines are directed at right angles to the wind direction. The model also

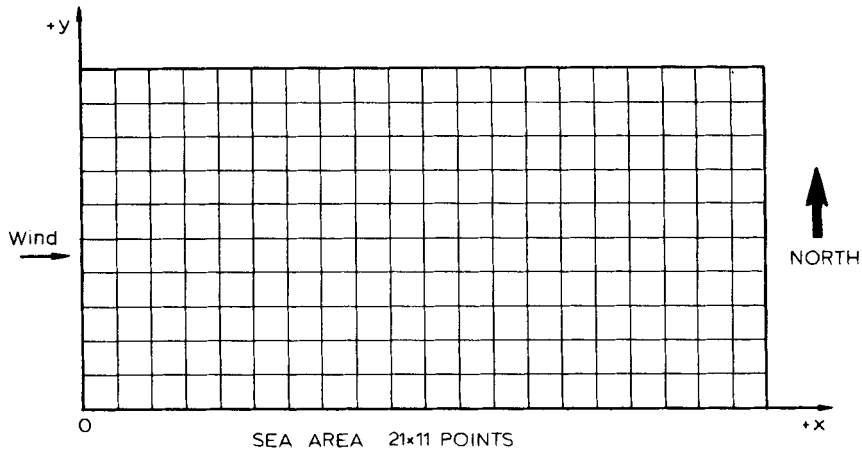

Figure 14. Closed basin configuration

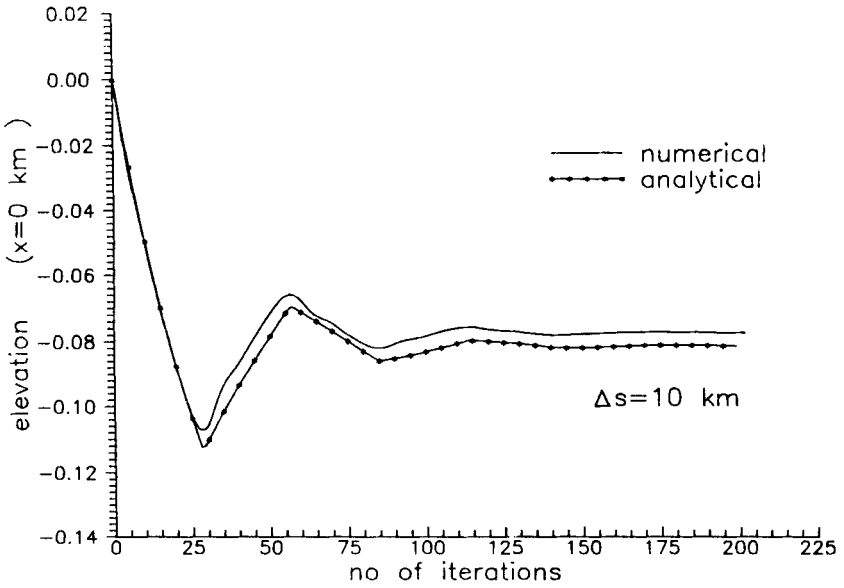

Figure 15. Time variation of elevation ζ at $x=0$, $y=B/2$

shows that the effect of the Coriolis force on the magnitude of the elevation is almost negligible and this agrees with Ekman's remark that 'the influence (of earth's rotation) on the absolute magnitude of the mounting up is rather moderate'.

In Figure 18 typical variations over the depth of the velocities u and v are given at the central point of the basin for two different kinds of A_z-distribution along the vertical axis. In the first case a constant eddy viscosity coefficient is assumed with a value of 0·0158 $m^2 s^{-1}$, while in the second case a parabolic distribution is introduced with zero values at the free surface at the bottom and

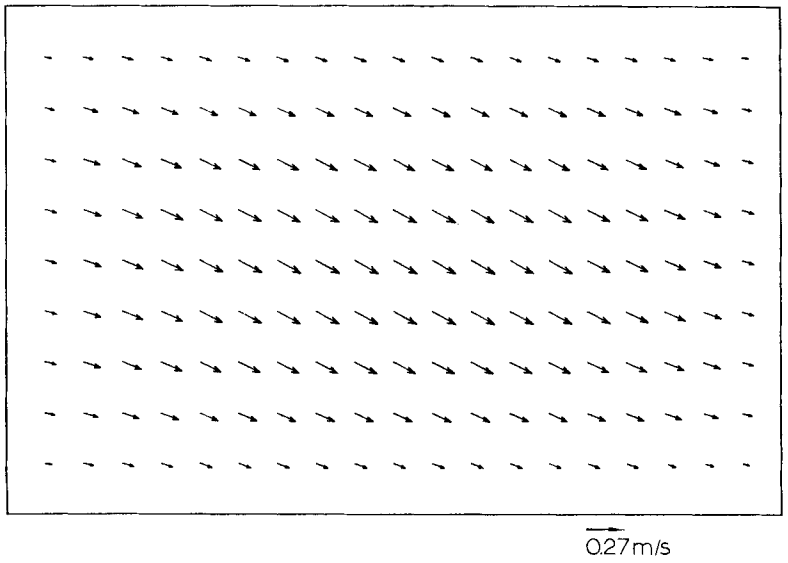

Figure 16. Closed basin—surface current

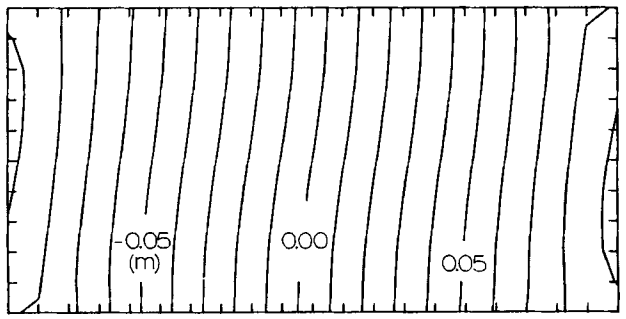

Figure 17. Closed basin—isolines of free surface elevation ζ

a maximum at half of the total depth (i.e. $h/2$) equal to 0·0158 $m^2 s^{-1}$. The results of the model show that this latter assumption does not lead to a plausible distribution of the velocities.

The same experiment as above is applied in the case of a basin communicating with the open sea along one of its sides. In this case specific 'absorbing' conditions must be defined along the open boundary line so that any disturbances generated inside the model propagate unhampered in the open sea without secondary reflections and other distortions along the boundary line which could probably return back and contaminate the numerical solution in the interior.

The results of such an application are shown in Figures 19–21. The mean velocities are again found equal to zero.

CONCLUSIONS

The method of characteristics is developed as a finite difference technique for the integration of the partial differential equations describing free surface flows propagating in an almost horizontal plane with negligible vertical accelerations.

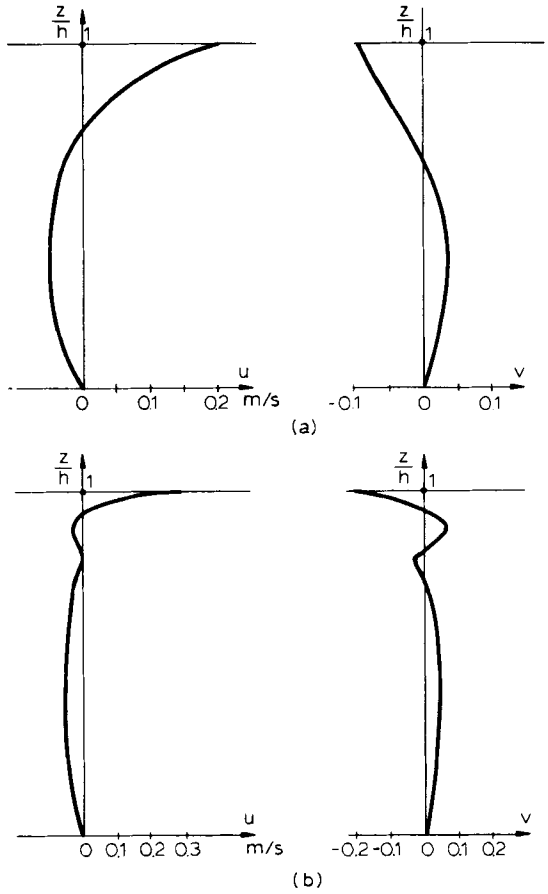

Figure 18. Vertical variation of u and v at centre of closed basin: (a) A_z constant; (b) A_z parabolic

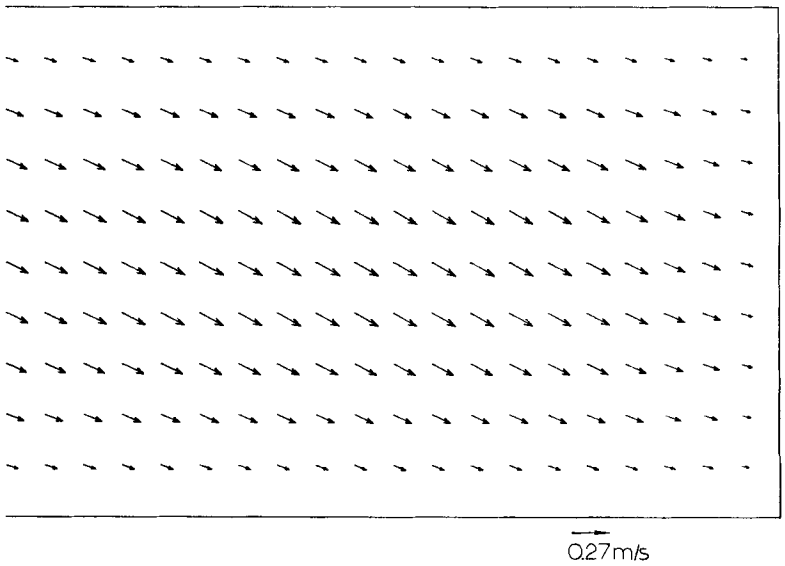

Figure 19. Open basin—surface current

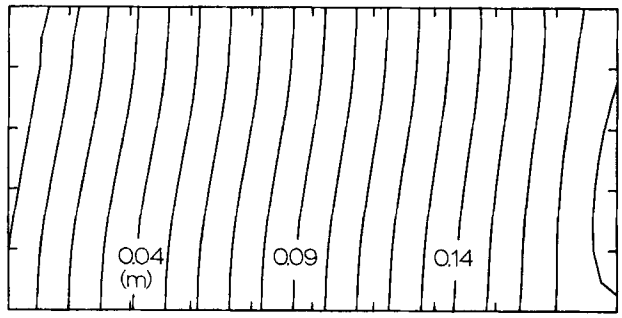

Figure 20. Open basin—isolines of free surface elevation ζ

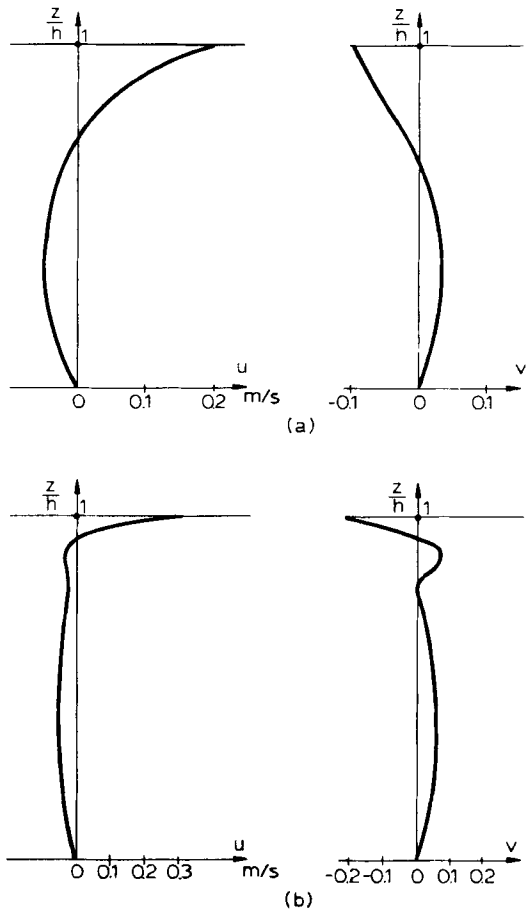

Figure 21. Vertical variation of u and v at centre of open basin: (a) A_z constant; (b) A_z parabolic

The method has the advantage of transforming the initial set of equations to the so-called characteristic conditions valid only along specific lines—the 'bicharacteristics'. These contain only total derivatives and thus may be directly integrated by using forward difference approximations. The resulting numerical scheme is of the explicit type and uses a non-staggered grid of solution points.

A two-dimensional, depth-integrated version of the scheme is applied for the simulation of tidal flow, which is a typical example of a nearly horizontal flow. Its performance is tested by comparing the results with a number of simple analytical solutions, e.g. the one developed by Lynch and Gray[19] for the case of a channel of a quarter-annular configuration and a quadratically varying depth. The scheme simulates accurately these analytical solutions. Subsequently, it is applied for the simulation of a real tide, namely that occurring in the Bristol Channel. The numerically produced isolines of tidal range and phase compare favourably with the observed values.

The 2D model is basically used for the calculation of the free surface elevation ζ using the mean depth values of the velocities U and V. Having done this, the gradient of the free surface is subsequently introduced into the three-dimensional equations to calculate the velocities u, v and w along the three axes x, y and z. This is achieved by defining the bottom shear stress directly from Newton's law of friction applied at the sea bottom. The partial derivatives involved in the bottom shear stress expressions are approximated by forward differences using the 3D solution of u and v.

This combined 2D–3D model is tested by using examples of wind-induced flow, e.g. that established inside a closed basin of constant depth by the action of a constant wind. For this case the classical Ekman solution is available for comparison. It is found that the model verifies all the main conclusions of Ekman's theory.

As a result of the above tests it is finally concluded that the three-dimensional model based on the method of characteristics may be considered as a reliable and accurate means for the simulation both in two and three spatial dimensions of a nearly horizontal flow under any kind of geometry and bathymetry conditions.

REFERENCES

1. J. P. Benque, J. A. Cunge, J. Feuillet, A. Hauguel and F. M. Holly Jr., 'New method for tidal current computation', *J. Waterway, Port, Coastal and Ocean Div. ASCE*, **108**, 396–417 (WW3), (1982).
2. N. S. Heaps, 'On the numerical solution of the three-dimensional hydrodynamical equations for tides and storm surges', *Mem. Soc. R. Sci. Liege, Ser. 6*, **2**, 143–180 (1972).
3. J. J. Leendertse and S. Lin, 'A 3-D model for estuaries and coastal seas, Vol. 2, Aspects of computation', *Rand Inst. Rep. R-1764-OWRT*, 1973.
4. G. Z. Forristall, 'Three-dimensional structure of storm-generated currents', *J. Geophys. Res.*, **79**, 2721–2929 (1974).
5. J. C. J. Nihoul, 'Three dimensional model of tides and storm surges in a shallow well-mixed continental sea', *Dyn. Atmos. Oceans*, **2**, 29–47 (1977).
6. A. A. Owen, 'A three dimensional model of the Bristol Channel', *J. Phys. Oceanogr.*, **10**, 1039–1050 (1980).
7. C. Koutitas and B. O'Connor, 'Modelling 3D wind induced flows', *J. Hydraul. Div. ASCE*, **106**, 1843–1865 (1980).
8. N. S. Heaps, 'Three-dimensional model for tides and surges with vertical eddy viscosity prescribed in two layers I. Mathematical formulation', *Geophys. J. R. Astron. Soc.*, **64**, 291–302 (1981).
9. M. C. Burg, Y. Coeffe and A. Warluzel, 'Tridimensional numerical model for tidal and wind generated flow', *Proc. 18th Coastal Engineering Conf. ASCE*, Capetown, 1982, pp. 635–651. ASCE, New York, 1983.
10. J. P. Benque, A. Hauguel and P. L. Viollet, *Engineering Applications of Computational Hydraulics, Vol. II, Numerical Models in Environmental Fluid Mechanics*, Pitman, London, 1980.
11. G. K. Furnes, 'A three-dimensional numerical sea model with eddy viscosity varying piecewise linearly in the vertical', *Continental Shelf Res.*, **2**, 231–242 (1983).
12. A. M. Davies, 'A three-dimensional model of wind-induced flow in a sea region', *Prog. Oceanogr.*, **15**, 71–128 (1985).
13. J. C. J. Nihoul and B. M. Jamart, *Three Dimensional Models of Marine and Estuarine Dynamics*, Elsevier, Amsterdam, 1987.
14. R. Courant, K. O. Friedrichs and H. Lewy, 'Uber die partiellen Differenzialgleichung der mathematischen Physik', *Math. Ann.*, **100**, 32 (1928).

15. D. S. Butler, 'The numerical solution of hyperbolic systems of partial differential equations in three independent variables', *Proc. R. Soc. Lond. A*, **225**, 232–252 (1960).
16. A. Daubert and D. Graffe, 'Quelques aspects des ecoulements presque horizontaux a deux dimensions en plan et non permanents: application aux estuaires', *La Houille Blanche*, **8**, 847–859 (1967).
17. P. F. Matsoukis, 'The analysis and application of the method of characteristics of simulating long wave propagation in the two-dimensional space', *Ph.D. Thesis*, Strathclyde University, Glasgow, 1980.
18. D. R. Lynch and W. G. Gray, 'Analytical solutions for computer flow model testing', *J. Hydraul. Div. ASCE*, **104**, (HY10), 1409–1428 (1978).
19. D. R. Lynch and W. G. Gray, 'A wave equation model for finite element tidal computations', *Comput. Fluids*, **7**, 207–228 (1979).
20. V. W. Ekman, 'On the influence of the earth's rotation on ocean currents', *Ark. Mat. Astron. Fys.*, **2**, 1–53 (11), (1905).
21. B. M. Jamart and J. Ozer, 'Numerical boundary layers and spurious residual flows', *J. Geophys. Res.*, **91**, 10621–10631 (C9), (1986).